UNIVERSITÀ DEGLI STUDI DI PADOVA

Dipartimento di Fisica e Astronomia

Corso di Laurea Triennale in Astronomia

A Primordial Black Hole origin of Planet 9 and its observability through dark matter indirect observations with the MAGIC telescopes

Relatore:
Prof. Alessandro De Angelis

Correlatore:
Dr. Rubén Lopéz Coto

Candidato:
Sara Fogliacco

ANNO ACCADEMICO 2020/2021

Contents

Abstract **1**

Introduction **1**

1 Theoretical background **4**

1.1 Dark Matter 4

1.1.1 Discovery and Confirmation 4

1.1.2 Gravitational Lensing 6

1.1.3 Candidate Particles 7

1.1.4 Primordial Black Holes 7

1.2 Planet 9 9

1.2.1 Planet 9 Hypothesis 10

2 Instrumentation **12**

2.1 MAGIC telescopes 12

2.2 Performance 13

2.3 Observability with MAGIC 18

3 Planet 9 as a Primordial Black Hole **22**

3.1 Why a PBH 22

3.2 Probability Distribution Function 24

3.3 Limits 26

4 Conclusion and Outlook **29**

List of Figures

1.1 Expected and observed rotation velocity for a galaxy. Observed one show that M∝r while expected one predicted v∝ $r^{-1/2}$. Observation are obtain by the studied of line 21 cm of neutral hydrogen. 5

1.2 The Optical Gravitational Lensing Experiment (OGLE) that runs a long-term variability sky survey. Its main goals are the detection and classification of variable stars, discovery of microlensing events, dwarf novae, and studies of the structure of the galaxy and the Magellanic Clouds. 6

1.3 Summary plot with new Nanograv bounds 9

1.4 The Outer Solar System, there are the orbit of distant dwarf planet (purple lines) and an hypothetical orbit for Planet 9 (orange line). The picture are not the best fit with our data, but it can explain the shape of our Solar System. 10

1.5 Table of 11 objects, that are stable or meta-stable with a>150 AU and q>42 AU. 11

2.1 MAGIC telescopes, Roque de los Muchachos Observatory. On left MAGIC-I is active since 2004, on right MAGIC-II is active since 2009 to significantly increase the sensitivity by stereo observations. MAGIC are the largest of the current Cherenkov telescope systems. Both instruments are made up of 270 individual mirror panels that can be independently focused using an active mirror control system equipped with lasers. 13

2.2 MAGIC telescopes, Roque de los Muchachos Observatory by night. A wide range of astrophysical questions is being investigated with MAGIC by observing highest energy, and cosmological aspects like Cold Dark Matter, Quantum Gravity effects and intergalactic magnetic fields. 14

2.3 Collection area of the MAGIC telescopes after the upgrade at the trigger level (dashed lines) and after all cuts (solid lines). Thick lines show the collection area for low zenith angle observations, while thin lines correspond to medium zenith angle. For comparison, the corresponding pre-upgrade collection areas are shown with gray lines. Image extracted from [5]. 15

2.4 Energy resolution (solid lines) and bias (dashed lines) obtained from the Monte Carlo simulations of gamma rays. Events are weighted in order to represent a spectrum with a slope of -2.6. Red: low zenith angle, blue: medium zenith angle. For comparison, pre-upgrade values are shown in gray lines. Image extracted from [5]. 16

2.5 Angular resolution of the MAGIC telescopes after the upgrade as a function of the estimated energy obtained with the Crab Nebula data sample (points) and Monte Carlo simulations (solid lines), 68% containment radius. Red points: low zenith angle sample, blue points: medium zenith angle sample. For comparison the low zenith angle pre-upgrade angular resolution is shown as gray points. Image extracted from [5]. 17
2.6 Differential (5 bins per decade in energy) sensitivity of the MAGIC Stereo system. We compute the flux of the source in a given energy range for which $N_{excess}/\sqrt{N_{bkg}} = 5$ with $N_{excess} > 10$, $N_{excess} > 0.05 N_{bkg}$ after 50 h of effective time. For better visibility the data points are joined with broken dotted lines. Image extracted from [5]. 18
2.7 The location of Planet 9 in galactic coordinates, the color scale indicates the culmination of that location in the sky at the MAGIC site. The red circle represents the location (RA/Dec) for P9. 19
2.8 Sky map, declination [deg] against right ascension [hours] of an example observation of the MAGIC telescopes, to convert degree into hours 1h=15deg. . . 20
2.9 Sky map of our search area. 21

3.1 The sky density plane, right ascension RA (x-axis) against semi-major axis a (y-axis). The black dot (45,380) is the most probable position of P9 in agreement with ours data. 25
3.2 The sky density plane, right ascension RA (x-axis) against predicted magnitude h (y-axis). The black dot (45,20) is the most probable position of P9 in agreement with ours data. 25
3.3 Comparison between sensitivity of CTA with other facilities. MAGIC blue dashed line, Fermi LAT green dotted line. The differential sensitivity shown below is defined as the minimum flux needed by CTAO to obtain a 5-standard-deviation detection of a point-like source, calculated in non-overlapping logarithmic energy bins, five per decade. Besides the significant detection, we require at least ten detected gamma rays per energy bin, and a signal/background ratio of at least 1/20. The analysis cuts in each bin have been optimised to achieve the best flux sensitivity to point-like sources. The optimal cut values depend on the duration of the observation. 26
3.4 *Fermi* Gamma-ray Space Telescope (FGST), the main instrument is Large Area Telescope (LAT) mostly intend to perform an all-sky survey studying astrophysical and cosmological phenomena such high-energy sources and dark matter. . . 27

Abstract

Over the past few years, there have been anomalies in the measured orbits of Trans Neptuinian and Kuiper Belt Objects that suggest the presence of a massive body in the outside of our Solar System. This measurements are also supported by the measurement of perturbation orbit of minor distant bodies and gravitational lensing events. This can be attributed to a body mass of $6.2^{+2.2}_{-1.3}$ $M_{\oplus}$, and there are two different hypotheses to explain its origin. The first one is that this body is the Planet 9, a distant and massive planet that has not been yet discovered due to its long orbit and low brightness; the second one, more interesting for us, that the object is Primordial Black Hole. This object orbits with a semi-major axis of 380^{+140}_{-80} AU and inclination of 16±5 deg. The presence of a Primordial Black Hole in our neighbour could be confirmed through annihilation signals from the dark matter microhalo around it. For this type of search it was suggested in the past that the *Fermi*-LAT gamma-ray satellite could be used and limits in the dark matter annihilation cross section were established using results from this satellite. In this thesis we have explored the possibility of extending these studies to the very-high-energy gamma-ray energy range using the MAGIC telescopes.

Introduction

Universe is made of matter, that is divided into baryonic (or normal) and **dark matter**. Together they are about 30% of energy-matter content of Universe.[1] Dark matter, unlike the baryonic one, does not interact with the electromagnetic field, for this reason it is hard to spot and detect. We can only study dark matter with gravitational effects on other matter. Several theories are born to understand this unknown particle, candidates for this hypothetical particle are axions, sterile neutrinos, weakly interacting massive particles (WIMPs), strongly interacting massive particles (SIMPs) and so on.

Astroparticle physics has the purpose of study elementary particles of the Universe and their interaction with fields. In particular a current unsolved problem is related to dark matter. To understand elementary particles we study their high energy spectrum. The Earth is bombarded by very high-energy particles coming from extraterrestrial sources, that were named *cosmic rays*.

Gamma rays consists of a short wavelength electromagnetic wave and very high energy photons. They generate in very high energy processes such as radioactive decay of atomic nuclei, particle annihilation or decay, synchrotron emission, bremsstrahlung, inverse Compton scattering, or pion decay. They provide information about the most energetic phenomena in the Universe and can be studied with satellites like *Fermi*-LAT or Imaging Atmospheric Cherenkov Telescopes like MAGIC, VERITAS, HESS or the future Cherenkov Telescope Array (CTA).

CTAs are a new generation of ground-based gamma-ray instruments in the energy range extending from some tens of GeV to about 300 TeV. Current gamma ray instruments like Fermi Large Area Telescope (LAT) in space, the ground-based Cherenkov telescope MAGIC, H.E.S.S. and VERITAS, the new generation water Cherenkov detector HAWC, are sensitive to overlapping and complementary dark matter particle mass ranges from $\sim$ 1GeV to $\sim$ 100TeV. One of them is the Major Atmospheric Gamma Imaging Cherenkov telescope (MAGIC) situated at the Roque de los Muchachos Observatory on La Palma (28.8°N, 17.9°W), one of the Canary Islands. MAGIC sensitivity to gamma rays is between 50 GeV and 50 TeV photon energy (very high energy). It achieves high sensitivity to Cherenkov light and low energy threshold domain. Its aim is to detect and study primary photons coming from, for example, the annihilation of dark matter. Instead, Fermi-LAT is a pair conversion telescope that is sensitive to gamma rays in the energy range from 20 MeV to 300 GeV, and it is able to efficiently survey the entire sky.

In this thesis, we studied the hypothetical Planet 9 (P9) as a **Primordial Black Hole** (PBH) to search dark matter through indirect observation with the MAGIC telescopes. If there is a P9 at a distance of hundred AU (Astronomic Units) from the Sun, it can explain several anomalies seen in Trans Neptunian Objects (TNOs) and in Kupier Belt Objetcs (KBOs). These

[1] the remaining part is Dark Energy.

objetcs, like Sednoidis, are to much distant form Neptune to be affected by its gravitational field. Other anomalies as microlensing events are observed by OGLE (Optical Gravitational Lensing Experiment) during last few years. They can be explain by a massive object (5-20 $M_{\oplus}$) with a semimajor axis of about 300-1000 AU.

1. Theoretical background

In this section we are going to show the theoretical basis of Dark Matter (DM), Primordial Black Holes (PBHs), and the hypothesis of Planet 9 (P9) as an introduction to the work performed in the thesis.

1.1 Dark Matter

Recently, measurements demonstrate that nearly 85% of the Universe's matter density is dark. The *Standard Model*[1] of particle physics alone cannot explain the nature of this DM. Unlike baryon matter, DM does not interact whit electromagnetic field, so it is call dark. It is invisible and undetectable by ordinary telescopes. DM and *Dark Energy*[2] are the most fascinated unsolved questions of modern physics and astrophysics.

The existence of a non-baryonic, neutral and cold dark matter component in the Universe is supported by an overwhelming body of observational evidence. There involved mainly the gravitational effect on the dynamics of cosmic structures like galaxy clusters, spiral galaxies and on the power spectrum of temperature anisotropies of the cosmic microwave background. There exist many theories beyond the Standard Model postulated about this new neutral, stable and weakly interacting massive particle with mass in the TeV scale, that could account for the measured DM relic density.[3]

1.1.1 Discovery and Confirmation

Hypothesis of DM was born in the beginning of the 20^{th} century (in 1933) with astrophysicist Zwicky. He applied the viral theorem[4] to galaxy clusters (in particular Coma Cluster $\sim$ 100 Mpc away) and he found something missing. Zwicky observed that the galaxies of the Coma Cluster were moving too fast for the cluster to be bound together by the visible matter of its galaxies. He called this missing mass **Dark Matter** (*Dunkle Materie* in German). This matter, unlike normal one, cannot be detected with electromagnetic interaction. DM interacts only with the gravitational field, although it is hypothesized to also interact with the Weak or Strong one. After Zwicky, several scientists tried to prove the existence of DM. In the 70's, astrophysicists Rubin, Ford, and Freeman provided strong evidence for the studied of rotation curve of galaxies. Indeed, the edge of the galaxy has velocity unsolved anomalies. The observed velocity

[1] is the theory describing three of the known fundamental forces (the electromagnetic, weak and strong interactions, gravity) in the universe, as well as classifying all known elementary particles.

[2] is an unknown form of energy that affects the universe on the largest scales, in agreement with the expansion of the universe.

[3] it is the density of a specific particle at the time of freeze-out.

[4] it provides a general equation that relates the total kinetic energy with the total potential energy of the system.

distribution does not correspond to the estimated one. The presence of invisible mass can fix this problem. From standard Newtonian gravity, we know the velocity of a star that moves in a circular trajectory around the galactic centre, with the following relation:

$$v(r) = \sqrt{\frac{GM}{r}}$$

where G is the gravitational constant [5], M is the enclosed mass and r is the radial distance. Follow the *Gauss's Law* for distance that extend beyond the galactic disk $v \propto r^{-1/2}$. The observation find, instead, that the circular velocity curve flattens out, that means M(r)∝r (see figure [1.1]). This is the stronger prove for the existence of DM.
Also the rate of mass-luminosity for a galaxy shows the presence of non-visible matter. An high value for $\frac{M}{L}$ means that there is a mass that does not emit electromagnetic waves.

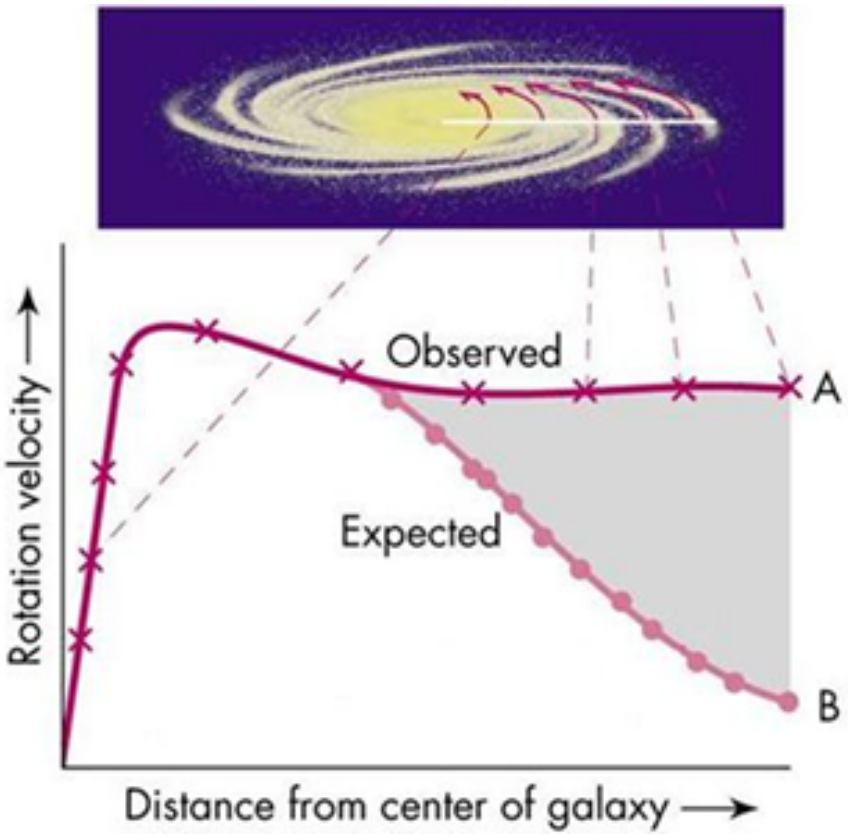

Figure 1.1: Expected and observed rotation velocity for a galaxy. Observed one show that M∝r while expected one predicted v∝ $r^{-1/2}$. Observation are obtain by the studied of line 21 cm of neutral hydrogen.

[5] G= $6.67 \times 10^{-11} \mathrm{m^3 kg^{-1} s^{-2}}$

1.1.2 Gravitational Lensing

Also *gravitational lensing* support the theory of DM. In agreement with General Relativity, the space-time is bent by gravity (i.e. mass). The effect has been proposed by Einstein (in 1936). It means that the light is deflected by a massive object (lens) as it travels from the source to the observer. The presence of DM can make visible the distant light sources behind.
There exist different types of lensing: strong, flexion, weak and microlensing. The classification depends on the concentration of mass. For example, microlensing happens when a small object crosses the line of sight of the source. It appears as a small increase in the observed luminosity. It is used to search for Jupiter-like objects.

Figure 1.2: The Optical Gravitational Lensing Experiment (OGLE) that runs a long-term variability sky survey. Its main goals are the detection and classification of variable stars, discovery of microlensing events, dwarf novae, and studies of the structure of the galaxy and the Magellanic Clouds.

Microlensing effect is in our interest because OGLE (see the picture [1.2]) experiment observed such anomalies. It can be explained by the presence of a massive body beyond Neptune's orbit, we are going to analyse this in the follower chapter.

1.1.3 Candidate Particles

It is natural to make the hypothesis that DM is also made out of elementary particles like ordinary matter. We have to fulfil the gravitational effect, the absence of electromagnetic interactions and strong interactions, the presence of weak interaction, they have to be stable or long-lived (they did not decay until today) and be cold/warm (non-relativistic motion). The most reliable theory shows that DM is formed of stable massive non-relativistic particles. [22]

The most reliable candidates are *Weakly Interact Massive Particles* (WIMPs), sterile neutrinos, Supersymmetric particles (SUSY) and axions.

WIMPs are favoured ones because they naturally have the right abundance to account for the DM, they were in equilibrium with the thermal plasma (high temperature in the early Universe), and then they *freeze-out* when the Universe expanded. Also superheavy WIMPs are proposed, they have masses around $10^{12} - 10^{16}$ GeV because the observation of ultra-high energy cosmic ray. That particles cannot be studied by accelerators directly. If they are stable, their existence can be probed by cosmological tests, but there is no direct link between astrophysical data and existence of superheavy metastable particles.

SUSY was proposed by Wess and Zumino (1973) and these particles can unify of electromagnetic weak and strong interaction. R-parity [6] prevents the proton to decay and makes the lightest SUSY particle (LSP), sneutrino, neutralino, and gravitino are proposed.

In quantum mechanics there is no reason to conserve CP (charge-parity), but experimental bounds on the neutron electric dipole moment indicate very small CP violations. Peccei and Quinn solved this issue with the postulation new symmetry (1977), axion particles appear when this symmetry is spontaneously broken. Axion has been product in the early Universe. Thermal production would give hot DM and non-thermal one (vacuum realignment, string decay and wall decay) make it possible to produce very cold axions. [18]

Additionally, primordial black holes are candidates for DM, we show why in the following section.

1.1.4 Primordial Black Holes

Primordial Black Holes (PBHs) are remnants of objects formed in the early Universe. They have a different origin from Black Holes (BHs), that formed after a collapse in a Super Novae event of massive star. PBHs are formed in the early universe (less than one second after Big Bang), when high densities and heterogeneous conditions could have led sufficiently dense regions to undergo gravitational collapse, that implies metric fluctuations. The simplest way to describe first order phase transitions with bubble creation in the early Universe is based on a scalar field theory with two non degenerated vacuum states. They were formed during

[6] R-parity is a concept in particle physics, it has a value of +1 for Standard Model particles and -1 for their superpartners.

a radiation-dominated phase[7] (thus non-baryonic), so they are candidates for DM. The first physicist studied and proposed PBHs was Hawking (in 1974). [13]

PBHs belong to the class of massive compact halo objects (MACHOs), they have a mass range $10^{-5} - 10^{50}$ g. Those smaller than 10^{15} g would have evaporated by now due to Hawking radiation. PBHs larger than this limit are subject to a variety of constraints associated with gravitational lensing, dynamical effects, in influence on large-scale structure, accretion and gravitational waves.

Their lifetime can be estimated by the Hawking radiation mechanism for BH. PBHs radiate as BHs (stars originated) and have a similar nature. This radiative process causes the BH to lose mass over time, with a remaining lifetime that depends on its mass. Differently than stellar BHs, the PBHs's birth mass is related to the *time of formation*. [11]

$$M \sim \frac{c^3 t_H}{G} = \Big(\frac{t_H}{10^{-23}\mathrm{s}}\Big) 10^{15}\mathrm{g} \tag{1.1}$$

where c[8] is the speed of light, t_H is the time of formation and G is the gravitational constant. PBHs can attract matter as any other BH, and if PBHs are in dense environments, the accretion could have been significant, especially for massive ones. There exist a relation between the *mass* and the *temperature* of a PBH.

$$T(M) = \frac{\hbar c^3}{8\pi G k}\frac{1}{M} \sim 100\Big(\frac{10^{15}\mathrm{s}}{M}\Big) \qquad [\mathrm{MeV}] \tag{1.2}$$

where M is the mass, $\hbar$ [9] is the reduced Planck's constant, k [10] is the Boltzmann constant. If the mass is above 5 $M_\oplus$ a PBH has a Hawking temperature of 0.004 K, it is colder than the cosmic microwave background (CMB, today T_{CMB}=2.728 K). The temperature increases over time as long as the mass is lost and from this it is possible to evaluate the *evaporation time*

$$\tau(M) = \frac{G^2 M^3}{\hbar c^4} \sim 10^{10}\Big(\frac{M}{10^{15}\mathrm{g}}\Big)^3 \qquad [\mathrm{yr}]. \tag{1.3}$$

If a PBH has an initial mass of around 10^{15} g, it would be evaporating today, producing an increasing emission, culminating with a disruption and a burst of *Very-High-Energy* (VHE) gamma-ray radiation.

It is in our interest because a PBH can emit a non-negligible part of DM. The expectation for the ray spectrum says that there are two components, the former one coming directly from Hawking radiation, thus peaking at around the PBH mass; and the last one, coming from the decay of hadrons produced in the fragmentation of primary quarks and gluons, peaking at lower energies. [3]

[7] most of the energy was in the form of radiation and that radiation was the dominant influence on the expansion of the universe.

[8] c =3×10^8 m/s

[9] $\hbar = \frac{h}{2\pi}$=6.58×10^{16}eV s

[10] k = $1.38\times10^{-23}\mathrm{m^2 kg\cdot s^{-2} K^{-1}}$

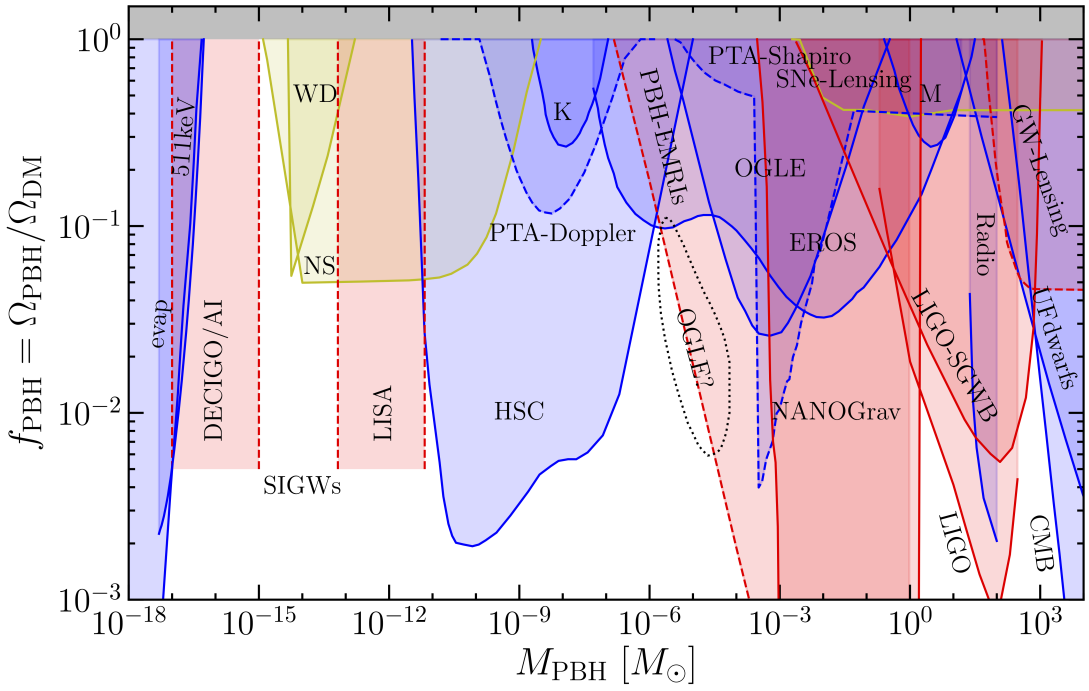

Figure 1.3: Summary plot with new Nanograv bounds

1.2 Planet 9

The search for planets in our Solar System is one of the most interesting topics for astrophysicists. Anyone who looks up at the sky is fascinated by the unknown. Solar System includes eight planets from Mercury to Neptune, and since Pluto has been downgraded as dwarf planet[11] scientists started to find a new *Planet 9* (P9). During past twenty years several minor bodies are discovered. They are divided into Trans Neptunian Objects (TNOs) that are bodies with semimajor axis greater that 30 AU (also Pluto belongs to); Kuiper Belt Objects (KBOs) and more distant Oort Cloud objects. Astrophysicist found *dwarf planet* like Makemake, Haumea, Eris, and so on (see figure [1.4]).

At the beginning of 2016, Caltech researchers revealed that they found evidence of a giant planet tracing a bizarre, highly elongated orbit in the outer Solar System (over 100 AU).[16]

[11] is a body that orbits the Sun, has enough mass to assume a nearly round shape, has not cleared the neighborhood around its orbit.

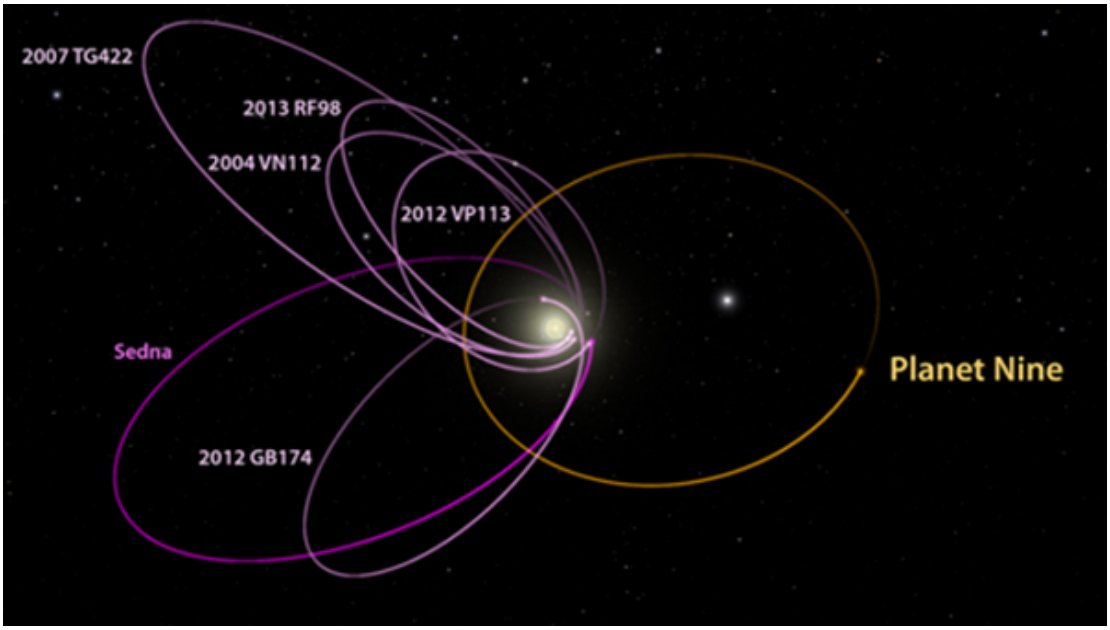

Figure 1.4: The Outer Solar System, there are the orbit of distant dwarf planet (purple lines) and an hypothetical orbit for Planet 9 (orange line). The picture are not the best fit with our data, but it can explain the shape of our Solar System.

1.2.1 Planet 9 Hypothesis

There are several evidence in agreement with P9. Sednoidis have a perihelion far removed from Neptune, that requires the presence of a past or current external perturber. The recent discovery of a Sedna-like body (2012VP113[12]) a potential additional member of the inner Oort Cloud, it pointed out a set of KBOs that exhibits unexplained clustering in orbital elements. In particular they have arguments of perihelia ω approximately around zero ($\omega \approx 0$). That means that the object's perihelion lies precisely at the ecliptic. This orbital grouping is surprising because gravitational torques exerted by the giant planets are expected to have random values. It suggests that there is an external perturbing bodies that makes ω=0 via the Kozai mechanism.[13] These bodies are too far away from Neptune so they are decoupled from its gravitational interactions. [6]

[12] is the farther known object that orbits the Sun.

[13] is a dynamical phenomenon affecting the orbit of a binary system perturbed by a distant third body causing the orbit's argument of pericenter to oscillate about a constant value.

name	a	e	i	Ω	ϖ
	AU		deg.	deg.	deg.
2000CR105	218	0.80	22.8	128.3	85.0
2003VB12	479	0.84	11.9	144.3	95.8
2004VN112	319	0.85	25.6	66.0	32.8
2010GB174	351	0.86	21.6	130.8	118.2
2012VP113	258	0.69	24.1	90.7	24.2
2013FT28	312	0.86	17.3	217.8	258.3
2013RA109	458	0.90	12.4	104.7	7.5
2013SY99	694	0.93	4.2	29.5	61.6
2013UT15	197	0.78	10.7	192.0	84.1
2014SR349	302	0.84	18.0	34.8	15.7
2015RX245	412	0.89	12.1	8.6	73.7

Figure 1.5: Table of 11 objects, that are stable or meta-stable with a>150 AU and q>42 AU.

To explain these anomalies for TNOs, astrophysicists hypothesized a P9 with a mass between 5 $M_\oplus$ and 20 $M_\oplus$ orbiting the Sun at a distance of 300-1000 AU. The existence of a massive, inclined and eccentric planet has been shown to be able to cause multiple dynamical effects, including a clustering of the longitude of the perihelion $\tilde{\omega}$ and of pole position (a combination of longitude ascending note Ω and inclination i). Analyses show that objects with q<42 AU are unstable (q is the perihelion), while all objects with q>42 AU are stable or meta-stable. There are 11 KBOs with a>150 AU (a is semimajor axis) and q>42 AU that have a longitude of perihelion clustered between 7°<$\tilde{\omega}$<118°, see figure [1.5].
The orbit of P9 is far away from the Sun, with high eccentricity and high inclination. Therefore, the initial range is

$$a \in [150,500]\,\text{AU} \qquad p \in [30,300]\,\text{AU} \qquad i \in [0,25]\,\text{deg} \qquad e \in [0.10,0.70]\,.$$

Another phenomenon that could dilute the clustering caused by P9 are the objects that are scattered inward from the inner Oort Cloud. Therefore, all objects with a>1000 AU are excluded. [14] Accurate analysis, reducing the range, shows that the orbital parameters are

$$a \in [300,460]\,\text{AU} \qquad p \in [240,385]\,\text{AU} \qquad i \in [11,21]\,\text{deg}.$$

For several assumptions, P9 is closer and brighter than initially expected, although the probability distribution includes a long tail to larger distances, and uncertainties in the radius and albedo of Planet Nine could yield fainter objects. [15]

2. Instrumentation

The *IACT* technique (Imaging Atmospheric Cherenkov Telescopes) is a method to detect very high energy (VHE) gamma ray photons in the energy range of $\sim$50 GeV to $\sim$50 TeV. They opened a new astronomical window to observe the gamma ray sky. Nowadays, there are four instruments: High Energy Stereoscopic System (H.E.S.S.), Major Atmospheric Gamma Imaging Cherenkov Telescopes (MAGIC), First G-APD Cherenkov Telescope (FACT), and Very Energetic Radiation Imaging Telescope Array System (VERITAS). The Cherenkov Telescope Array (CTA) is a multinational project to build next-generation IACTs.
The IACT uses one or more optical telescopes that image the air showers induced by cosmic gamma rays in the atmosphere through the *Cherenkov radiation* produced by the ultra-relativistic charged particles. The annihilation of positron and electron (e^+e^-) create a flask of light. The light, produced by Cherenkov radiation from the charged particles of the atmospheric shower, travel faster than the light in the air. This faint light flash can be detected above the ambient, generally lasting just a few ns (10^{-9}s). Most of this light is emitted at altitudes ranging between 5 to 15 km. Above a few TeV, Cherenkov light from electromagnetic showers becomes significantly brighter, at the same time, the gamma-ray flux decreases with energy, so to detect a sufficient number of these high-energy events, a large ground surface needs to be covered.

2.1 MAGIC telescopes

MAGIC telescopes are a system of two 17m diameter imaging atmospheric Cherenkov telescopes located at the Roque de los Muchachos Observatory (La Palma, Canary Island) at an altitude of 2200 a.s.l. The first telescope, MAGIC-I, is in operation since 2004. The second one, MAGIC-II, was built in 2008 at a distance of 85m from the first. Both mirrors have a collecting area 236 m^2. They achieve the best performance for VHE gamma ray observation in the absence of moonlight. The two MAGIC telescopes can be operated independently or in stereoscopic mode, the second one allows a more precise reconstruction. Between 50GeV and 150GeV, MAGIC telescopes have the best sensitivity of the current IACT.
MAGIC telescopes are a stereoscopic system of two IACTs, see Figures [2.1,2.2], it is one of the most sensitive currently operating instruments.

Detailed Monte Carlo simulations are required to estimate the performance of an IACT array, which is evaluated by quantities like the minimum detectable flux sensitive FoV (field of view) or its angular and energy resolutions. [10]
It is possible to identify the nature of the primary particle and reconstruct its original energy and incoming direction. These types of instruments work only at night and preferentially during dark moonless conditions. Therefore, the cameras of the MAGIC telescopes were designed from the beginning to allow observation during moderate moonlight [9].

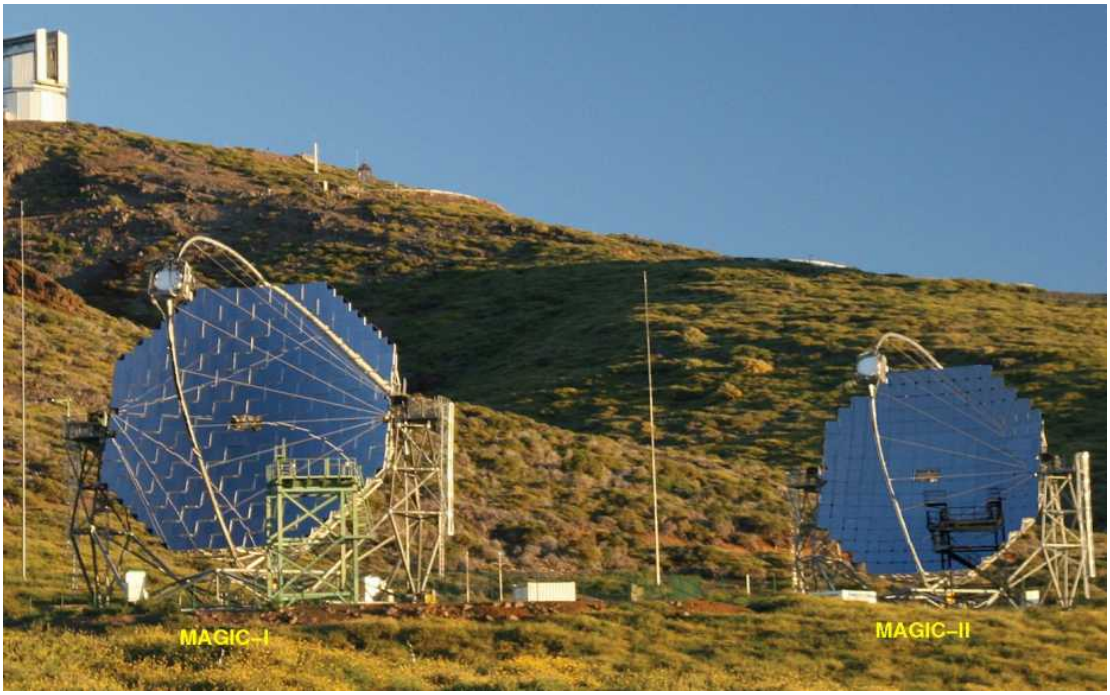

Figure 2.1: MAGIC telescopes, Roque de los Muchachos Observatory. On left MAGIC-I is active since 2004, on right MAGIC-II is active since 2009 to significantly increase the sensitivity by stereo observations. MAGIC are the largest of the current Cherenkov telescope systems. Both instruments are made up of 270 individual mirror panels that can be independently focused using an active mirror control system equipped with lasers.

Gamma rays of different origins have different spectral shapes, DM-induced emission is characterized by a peculiar cut-off for energy and other remarkable spectral features, while other sources have a plain spectral shape. MAGIC is sensitive to cosmic gamma rays with photon energies between 50 GeV and 30 TeV, other ground-based gamma-ray telescopes typically observe gamma energies above 200–300 GeV. This means that MAGIC can cover an enormous energy spectrum. [1]

2.2 Performance

MAGIC telescopes are in a commissioning phase since 2003. Beyond technical runs, there was time also for some physics observations. Both kinds of runs were necessary to tune or improve the hardware of the detectors, and the first physics signals were ready in 2004. The first sources observed were the Crab Nebula and Mkn 421, they are a sort of standard sources. [23]

After the fraction of gamma ray observable is determined, it is possible to estimate how many gamma rays can be actually observed. The number of σ can be calculated using the

Li-Ma formula, [4] [21],

$$N_\sigma = Q\frac{(R_{on}-R_{off})T}{\sqrt{(R_{on}+R_{off})T}} = Q\frac{R_\gamma\sqrt{T}}{\sqrt{R_{on}+R_{off}}} \tag{2.1}$$

where Q is the quality factor (the efficiency of the analysis of order unity as low energy), T is the actual acquisition time and the R's represent the rates. They take into account the particle flux ϕ and the detector sensitivity to the flux expressed as the effective area of telescope A_{eff}.

$$R_\gamma = \int \phi_{GR}(E)A_{eff}(E,\theta)dE \tag{2.2}$$

Figure 2.2: MAGIC telescopes, Roque de los Muchachos Observatory by night. A wide range of astrophysical questions is being investigated with MAGIC by observing highest energy, and cosmological aspects like Cold Dark Matter, Quantum Gravity effects and intergalactic magnetic fields.

The energy threshold cannot be obtained in a straight-forward way from the data itself. One needs to rely on the Monte Carlo simulations and to make sure that they describe the data correctly. The energy threshold depends on the trigger settings for a given observation. A definition of an energy threshold is the peak energy of such a plot for a hypothetical source with a spectral index of -2.6. For MAGIC, the threshold value is determined by fitting a Gaussian distribution in a narrow range around the peak.

For large arrays the *collection area* well above the energy threshold for low zenith angle observation is roughly equal to the physical size of the array, while, for a single telescope (or small arrays) such as the MAGIC telescopes, the collection area is mainly determined by the size of the Cherenkov light pool.

$$A_{eff}(E) = \frac{N(E)}{N_0(E)}\pi r_{max}^2$$

This is the collection area as function of energy E, N_0(E) is the number of simulated events, r_{max} is the maximum simulated shower impact, and N(E) is the number of events surviving either the trigger condition. The collection area of the MAGIC telescopes at the trigger level is

about 10^5 m^2 for 300 GeV gamma rays, see [2.3]. It grows with energy in the range TeV. We also show the collection area after image cleaning, quality and signal extraction cuts optimized for best differential sensitivity. In observations at low zenith angles, the density of Cherenkov light photons on the ground produced by a VHE gamma ray shower depends mostly on its energy and its impact parameter. [5]

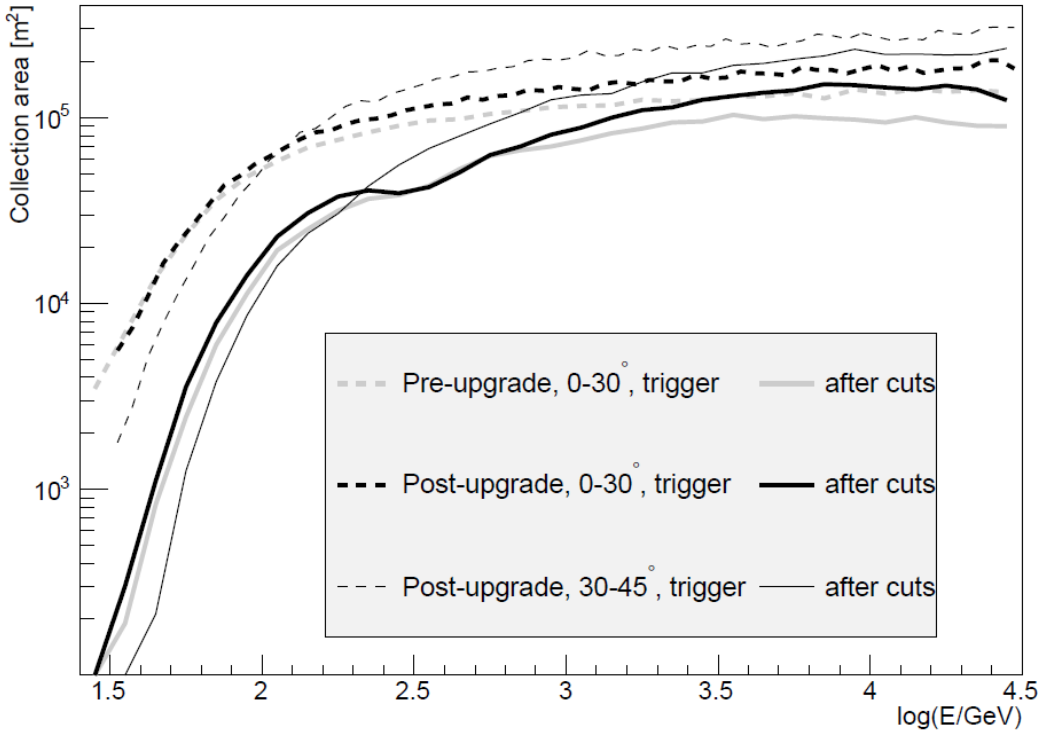

Figure 2.3: Collection area of the MAGIC telescopes after the upgrade at the trigger level (dashed lines) and after all cuts (solid lines). Thick lines show the collection area for low zenith angle observations, while thin lines correspond to medium zenith angle. For comparison, the corresponding pre-upgrade collection areas are shown with gray lines. Image extracted from [5].

The Monte Carlo simulations are divided into bins of true energy, in each bin we construct a distribution of $(E_{est} - E_{true})/E_{true}$ and fit it with a Gaussian function. The distribution is well described by a Gaussian function in the central region, but not at the edges, where one can appreciate non-Gaussian tails. Figure [2.4] there is the energy resolution and the bias of the MAGIC telescopes as a function of the true energy. At low energies (less than 100 GeV), the estimated energy bias rapidly increases due to the threshold effect. At low energies, the energy resolution is degraded due to worse precision in the image reconstruction and higher internal relative fluctuations of the shower. Above a few hundred GeV, the absolute value of the bias is below a few percent. The bias is corrected in the spectral analysis by means of an unfolding

procedure. [5]

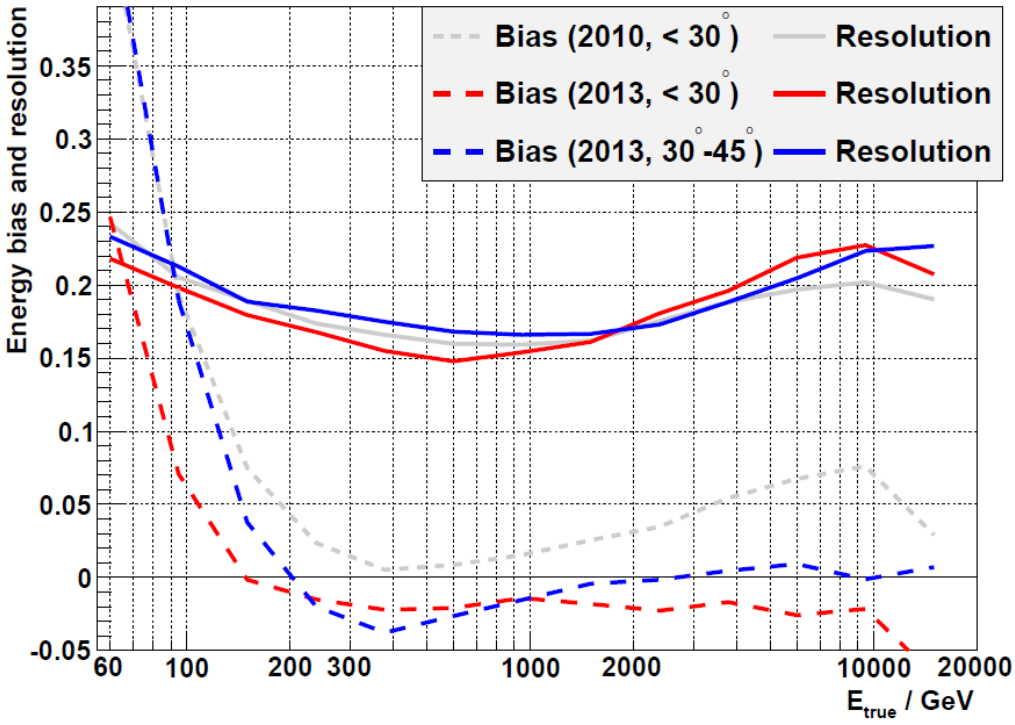

Figure 2.4: Energy resolution (solid lines) and bias (dashed lines) obtained from the Monte Carlo simulations of gamma rays. Events are weighted in order to represent a spectrum with a slope of -2.6. Red: low zenith angle, blue: medium zenith angle. For comparison, pre-upgrade values are shown in gray lines. Image extracted from [5].

To obtain the angular resolution, we use two methods. The former one defines the angular resolution Θ_{Gauss} as the deviation of a 2-dimensional Gaussian fitted, it is a good performance quantity for looking for small extensions; the latter one computes an angular distance $\Theta_{0.68}$ around the source, it is more sensitive to long tails in the distribution of reconstructed directions. Their absolute values are different, normally $\Theta_{Gauss} < \Theta_{0.68}$. Figure [2.5] shows the angular resolution obtained with the last method.

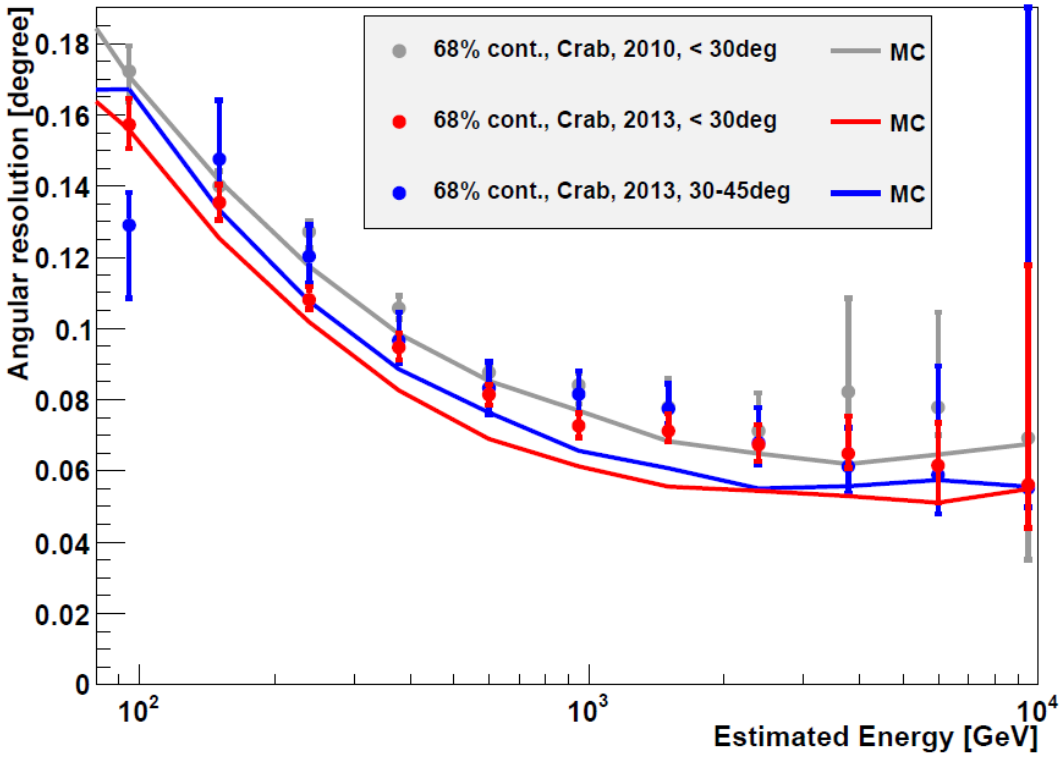

Figure 2.5: Angular resolution of the MAGIC telescopes after the upgrade as a function of the estimated energy obtained with the Crab Nebula data sample (points) and Monte Carlo simulations (solid lines), 68% containment radius. Red points: low zenith angle sample, blue points: medium zenith angle sample. For comparison the low zenith angle pre-upgrade angular resolution is shown as gray points. Image extracted from [5].

Following the commonly used definition, we calculate the sensitivity in narrow bins of energy. The differential sensitivity is plotted for low and medium zenith angles in image [2.6]. The sensitivity clearly depends on the observation time which can be spent observing a given source. In the medium range of observation times, the sensitivity follows the usual $\propto 1/\sqrt{time}$ dependence. While for very short observation times, especially for higher energies, the limiting condition of at least 10 excess events leads to a dependence of $\propto 1/time$. On the other hand, for very long observations the sensitivity saturates at low energies.

For a weak source, the significance of an excess of N_{excess} events over a well known background of N_{bkg} events can be computed with the simplified formula $N_{excess}/\sqrt{N_{bkg}}$. Therefore, the sensitivity $S(N_{excess}/\sqrt{N_{bkg}})$ is defines as the flux of a source giving $N_{excess}/\sqrt{N_{bkg}} = 5$ after 50 h of effective observation time. Another way to calculate the sensitivity is by using the Li-Ma [2.1], which is the standard method in the VHE gamma ray astronomy for the calculation of the significances. For a more realistic estimation of the sensitivity, it is necessary to

applay conditions N_{excess}>10, that assures that the Poissonian statistics of the number of events can be approximated by a Gaussian distribution, and N_{excess}>0.05 N_{bkg}, protects against small systematic discrepancies between the ON and OFF distributions. See [5]

Differential sensitivity of MAGIC, the flux of a source which gives after 50h of observations 5 σ signal, calculated according to Li-Ma formula [2.1], assuming 3 background regions in estimated energy bin E1-E2.[1]

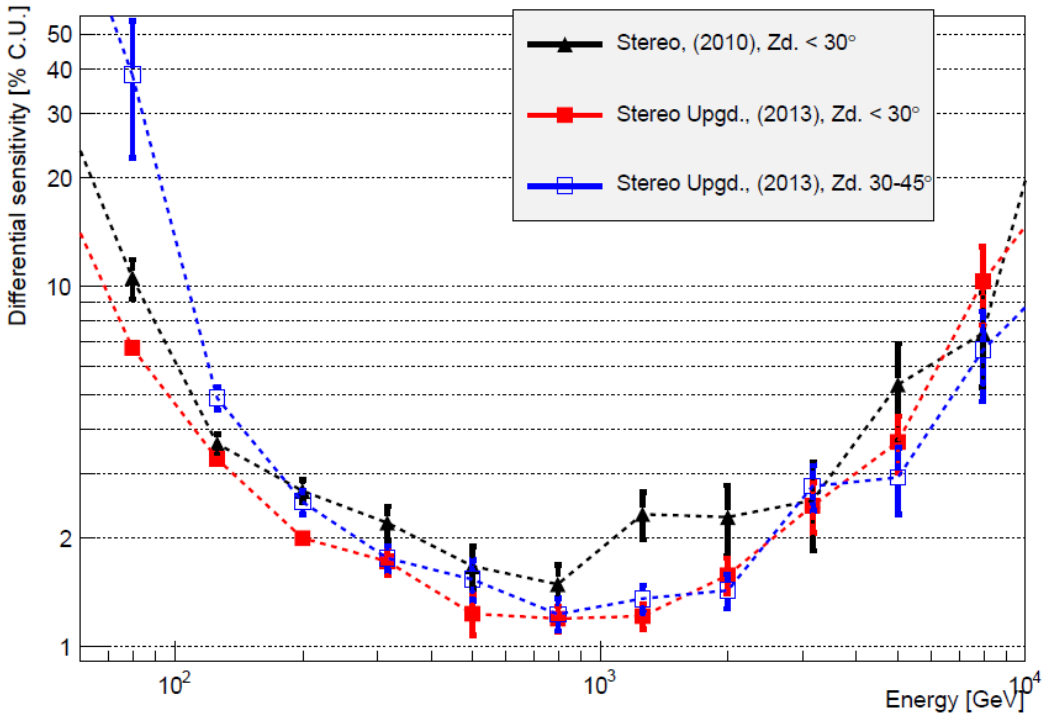

Figure 2.6: Differential (5 bins per decade in energy) sensitivity of the MAGIC Stereo system. We compute the flux of the source in a given energy range for which $N_{excess}/\sqrt{N_{bkg}} = 5$ with $N_{excess} > 10$, $N_{excess} > 0.05 N_{bkg}$ after 50 h of effective time. For better visibility the data points are joined with broken dotted lines. Image extracted from [5].

2.3 Observability with MAGIC

We know what *Fermi*-LAT can see, but about MAGIC? MAGIC telescopes have a range of energy photon of ∼30 GeV to ∼30 TeV, they have an higher level of energy than *Fermi*-LAT. Figure [3.3] shows several CTAs and compared their *differential flux sensitivity*. We will focus about MAGIC and *Fermi*-LAT, the plot can be distinguished in four areas. [2]

[1] https://magic.mpp.mpg.de/newcomers/technical-implementation0/

- For energies lower than $\sim 10^{-1}$TeV, *Fermi*-LAT has higher sensitivity than MAGIC telescopes.
- At $\sim 10^{-1}$TeV they have roughly the same sensitivity.
- For energies between $\sim 10^{-1}$TeV and $\sim$1 TeV, MAGIC telescopes have higher sensitivity than *Fermi*-LAT.
- For energies over $\sim$1 TeV *Fermi*-LAT cannot observe, but MAGIC telescopes range continue up to $\sim$10 Tev.

The best mass for our hypothetical P9 is $6.2^{+2.2}_{-1.3}$ $M_\oplus$ that means $\sim \left(\frac{125\text{GeV}}{T}\right)^2$ $M_\oplus$ [24]. With MAGIC telescopes we can study a bigger range and we can continue up to the order of 10 TeV, where *Fermi*-LAT had no access.
Best estimates for right ascension and declination are (in agreement with [15] and figures [3.1,3.2])

$$RA = 45\text{deg} \qquad \delta = 12\text{deg}$$

These are our sky coordinates, they indicate where we need to observe. Also with [2.7] we can understand where P9 is . The area that we interest to observe is the red one, in agreement with hypothesis. The *zenit* is the highest level reached by a body, P9 in our case. It is the direction of reference for measuring the zenith angle, the angle between the direction of interest and the local zenith. All objects in the sky can be projected upon the inner surface of the celestial sphere, the red dot is the "higher point" on the celestial sphere of P9.

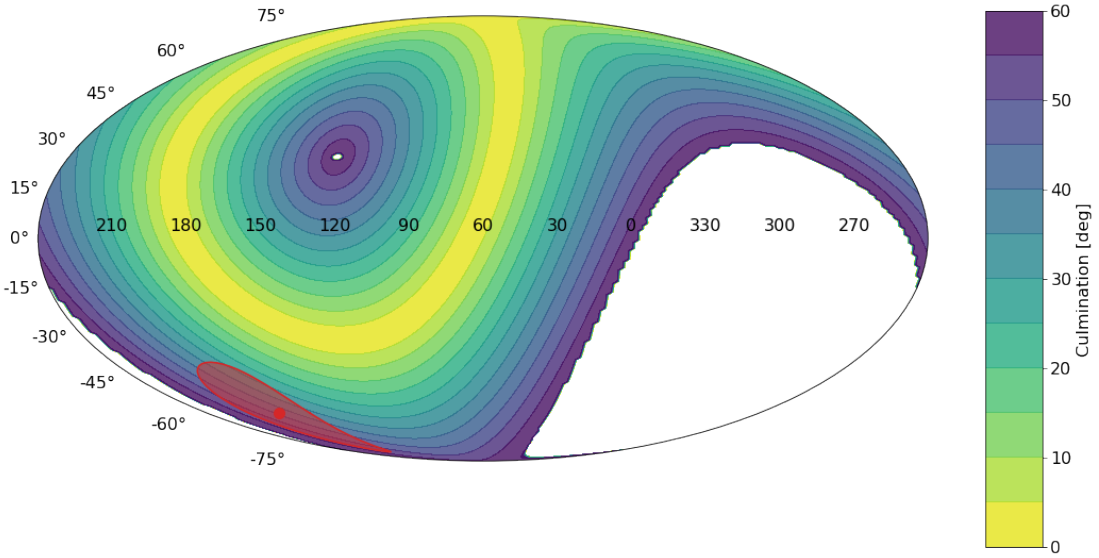

Figure 2.7: The location of Planet 9 in galactic coordinates, the color scale indicates the culmination of that location in the sky at the MAGIC site. The red circle represents the location (RA/Dec) for P9.

We have observation data through Data Level 3 (DL3), so we can analyse the observation time per given RA and δ. The file with data contains right ascension, declination and observation time, etc. Total observation time is 29 days 1 hour 14 minutes (2510112 s) for 2372 observations. While the observations we are focusing on are 156 with total amount of observation time $\sim$ 47 hours. It will be exposed in the following chapter in section 3.3.
To analyse our data we used *astropy* module of Python, *gammapy* is a package for gamma-ray, *healpy* is to handle pixelated data on the sphere.
Radius of uncertainty is 20 deg and the radius of MAGIC telescopes are $\sim$2 deg, we have a circular region in the sky with P9 as the center and 22 deg as the radius (sum of uncertainty radius and magic one).

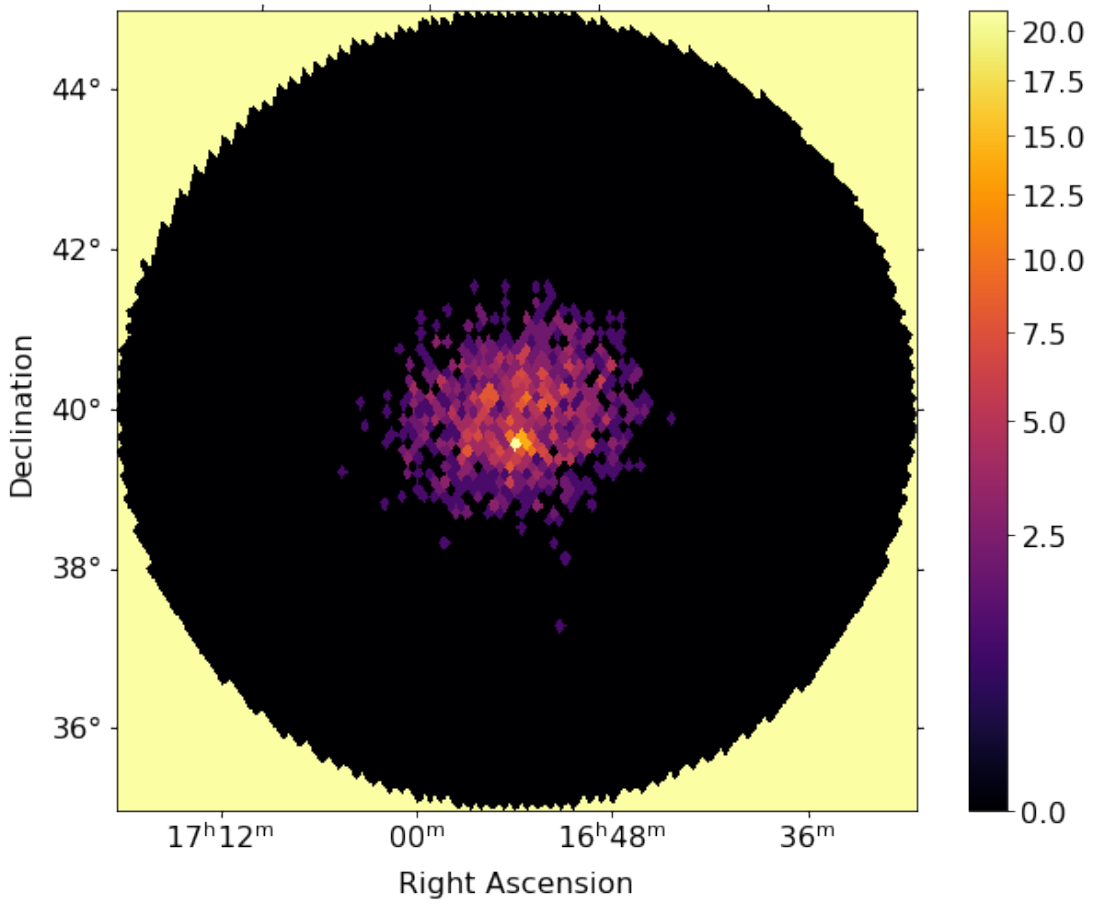

Figure 2.8: Sky map, declination [deg] against right ascension [hours] of an example observation of the MAGIC telescopes, to convert degree into hours 1h=15deg.

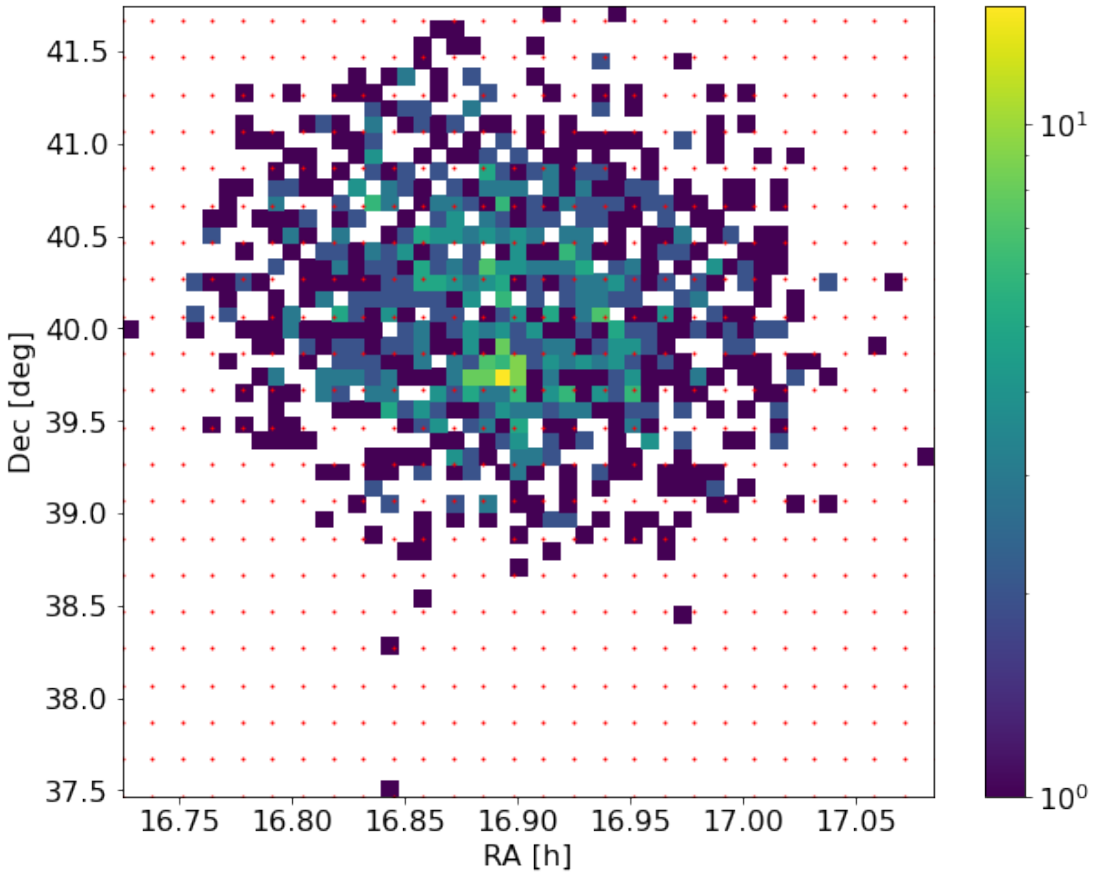

Figure 2.9: Sky map of our search area.

3. Planet 9 as a Primordial Black Hole

In addition to anomalies connected to the orbits of TNOs, there are another unexpected gravitational fact. The *Optical Gravitational Lensing Experiment* (OGLE) reported an excess of six ultra-short micro-lensing events with crossing times of 0.1-0.3 days. The lensing objects are located toward the galactic bulge (around 8 kpc away). These events correspond to objects of the same mass we assumed for P9 and it could be interpreted as a PBH. If P9 is a PBH, we can detect its DM microhalo forms around it. [24]

3.1 Why a PBH

Simulation and analytic arguments indicate that these observations can explain both anomalies in the predicted dynamics assuming the existence of a giant planet. To fix the gravitational parameters of TNOs P9, it would be enough, but the OGLE observations need a PBH. It are consistent with

$$M \in [0.5, 20]\,\mathrm{M}\oplus \qquad f_{PBH} \in [0.005, 0.1] \tag{3.1}$$

where $f_{PBH} = \frac{\Omega_{PBH}}{\Omega_{DM}}$ and $\Omega_{DM}\hbar^2 \approx 0.1$ are respectively density fraction and relic density. An object of $\sim \mathrm{M}_\oplus$ is too light to be a BH formed by stellar collapse. PBHs arise form early Universe and as a result can be lighter than $\mathrm{M}_\odot$. They are formed during *radiation domination* via a strong first order phase transition around the electroweak scale, they are expected to have mass of the order $M_{BH} \sim \left(\frac{125GeV}{T}\right)^2 \mathrm{M}_\oplus$ [1]. [19]
We assume DM account for the remaining fraction $f_{DM} = 1 - f_{PBH} \approx 1$ so $f_{PBH} \ll 1$. In this case, DM densities in microhalo are typically very high and DM annihilation can be significantly enhanced and potentially detectable. [20]

DM particles could form degenerate objects at earlier epochs, which provided a motivation to consider P9 to be such a DM object. It would not emit any radiation at any wavelength and therefore not to be seen in the usual observational searches. There could be just one object in the Oort Cloud volume, and hence in our galaxy there could be as many as 10^{15} objects like this.

The gamma ray flux produced by DM annihilation in a given region of the sky ($\Delta\Omega$) and observed at Earth is given by

$$\frac{d\Phi}{dE}(\Delta\Omega) = \frac{1}{4\pi}\frac{\langle\sigma v\rangle J(\Delta\Omega)}{2m_{DM}^2}\frac{dN}{dE} \tag{3.2}$$

$$J(\Delta\Omega) = \int_{\Delta\Omega} d\Omega' \int_{l.o.s} dl\,\rho^2(l,\Omega') \tag{3.3}$$

[1] By mass–energy equivalence, the eV is also a unit of mass E=mc^2.

where m_{DM} is the mass of the DM particle, $\langle\sigma v\rangle$ is the thermally-averaged annihilation cross section, dN/dE is the average gamma ray spectrum per annihilation reaction and J is the astrophysical factor (or J-factor) with ρ being the DM density and the integrals running over $\Delta\Omega$ and the line of sight (l.o.s) through the DM distribution.

Through our estimation for the mass of P9 $6.2^{+2.2}_{-1.3}$ $M_\oplus$ we can calculate the temperature and evaporation time of PBH with the equation [1.2] and [1.3]. Therefore, the PBH has a temperature of $\sim$0.0003 K and an evaporation time $\tau \sim$50 Gyr, this makes impossible to see the Hawking radiation because the timescale is too long (the Universe exists from $\sim$14 Gyr ago). However, the DM halo around PBH can provide a powerful signal if it annihilates. This source can be detected with MAGIC telescopes. The whole PBH contributes to gamma ray diffuse emission. We consider a "freeze-in" DM candidate, its relic density is

$$\sigma_{DM} \approx 0.2\Big(\frac{\mathrm{m}}{100\mathrm{GeV}}\Big)\Big(\frac{\lambda}{6\times10^{-12}}\Big)^2\Big(\frac{10\mathrm{TeV}}{M_\phi}\Big) \tag{3.4}$$

where the mass m coupled to a mediator state ϕ with mass M_ϕ, $\lambda \ll 1$

$$\langle\sigma v\rangle \approx \frac{\lambda^2 g^2 m^2}{\pi M_\phi^4}, \tag{3.5}$$

assume an annihilation cross section of standard model particles.
This implies a characteristic cross section of order

$$\langle\sigma v\rangle_{ch} \approx 1.3\times10^{-56}\mathrm{cm}^3/\mathrm{s}\times\Big(\frac{\mathrm{g}}{10^{-2}}\Big)^2. \tag{3.6}$$

.

OGLE indicates $f_{PBH} \ll 1$, PBHs accrete dense DM micrhohalos, in the rest is taken up by the DM component. In the absence of DM, it would be impossible to detect a PBH of this mass. We need to consider an initial configuration and the subsequent evolution to describe the DM profile around the PBH. We taken into account the radius of influence r_{in} that corresponds to the region in which the PBH dominates the local gravitational potential. In this radius there is DM mass equal to the PBH mass, the DM profile in the case for $M_{PBH} \geq M_\oplus$ and $m \geq$100 GeV.

$$M_{PBH} = \frac{4\pi}{3}\rho(t)r_{in}^3(t) \tag{3.7}$$

and

$$\rho(r) = \frac{\rho_{eq}}{2}\Big(\frac{r_{eq}}{r}\Big)^{9/4} \tag{3.8}$$

where $r_{eq} = r_{in}(t_{eq} \sim 220\ \mathrm{AU} \times (M_{PBH}/5M_\oplus)^{1/3}$ is the radius of influence at matter-radiation equality, $\rho_{eq} = \rho(t_{eq}) \approx 2.1\times10^{-19}$ g/cm^3 is the density of Universe at matter-radiation equality. If the DM can annihilate, the inner DM density may be depleted implying a cross-section-dependent region of constant density $\rho_{max} = \frac{m}{\langle\sigma v\rangle\tau}$ within a radius $r_{max} = r_{eq}\Big(\frac{\langle\sigma v\rangle\tau\rho_{eq}}{2m}\Big)^{4/9}$, where τ is the age of the Universe and $\langle\sigma v\rangle$ is the thermally average annihilation cross section. [8]

$$\langle\sigma v\rangle < 1.4\times10^{-54}\mathrm{cm}^3/\mathrm{s}\Big(\frac{m}{100GeV}\Big)\Big(\frac{M_{PBH}}{5M_\oplus}\Big)^{3/2} \tag{3.9}$$

3.2 Probability Distribution Function

A *probability distribution function* (PDF) is the integral of the probability density function and it can be interpreted as providing a relative likelihood. This function tells us about the probability of an event that will occur in a given interval. We used it to estimate with high precision the orbital parameters and to find its sky coordinates to detect P9. [15]

To estimate the orbitals parameters of P9, we require a likelihood model for a set of orbitals parameters given the data on the observed KBOs. We find semi-major axis of 380^{+140}_{-80} AU, inclination of $16\pm5°$ and perihelion of 300^{+85}_{-60}AU. These values are obtained by simulation with MCMC (Markov Chain Monte Carlo), an emulation of likelihood and Gaussian process. The random variables for this model are the mass of the planet m_9, the semi-major axis a_9, the eccentricity e_9, the inclination i_9, the longitude of perihelion $\tilde{\omega}_9$, and the longitude of ascending node Ω_9. Test particle is initially distributed with semi-major axis between 150 and 500 AU, perihelion between 30 and 50 AU, and inclination between 0° and 25°.

To estimate the PDF, we seek the probability of observing an object at $(i,\tilde{\omega},\Omega)$ given (a,e) for each simulation. Then a probability distribution function of the pole position $(\sin i\cos\Omega, \sin i\sin\Omega)$ has been created. The distribution from these simulations can be empirically fit by a *Fréchet distribution*[2] of the form

$$p(a) = (a-\mu)^{-(\alpha+1)} e^{(-\frac{a-\mu}{\beta})^{-\alpha})}$$

where $\alpha = 1.2$, $\beta = 1570$ AU and $\mu = -70$ AU.
At the end $a_9 = 300, 380, 520$ AU, that means 380^{+140}_{-80} AU, so the perihelion distance is 300^{+85}_{-60} AU and the aphelion distance is 460^{+200}_{-110} AU.
Distributions for the mass and orbital elements of Planet Nine now estimated, we are capable of determining the PDF of the on-sky location, the heliocentric distance, and the predicted brightness of P9. The most probable values for declination δ and right ascension RA are $\delta = 12$ deg and $RA = 45$ deg. Now it is also possible to estimate the magnitude of P9 and we need mass, diameter and albedo[3]. We assume that the most likely planetary composition is a icy-rocky core with H-He rich envelope to estimate the albedo, then it is ~ 0.75. For diameter we use a simple mass-diameter relationship of $r_9 = \left(\frac{m_9}{3M_\oplus}\right)\mathrm{R}_\oplus$. Data of RA and δ have been found in CalthecDATA[4] for Planet Nine reference population. [17]

[2] is a special case of the generalized extreme value distribution.

[3] is the measure of the diffuse reflection of solar radiation out of the total solar radiation and measured on a scale from 0, a black body that absorbs all incident radiation, to 1, a body that reflects all incident radiation.

[4] https://data.caltech.edu/records/2098

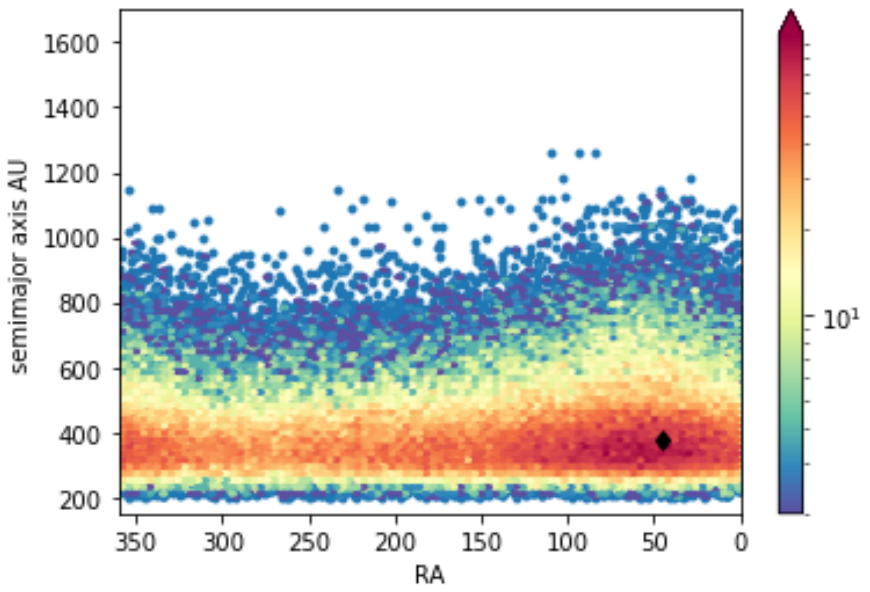

Figure 3.1: The sky density plane, right ascension RA (x-axis) against semi-major axis a (y-axis). The black dot (45,380) is the most probable position of P9 in agreement with ours data.

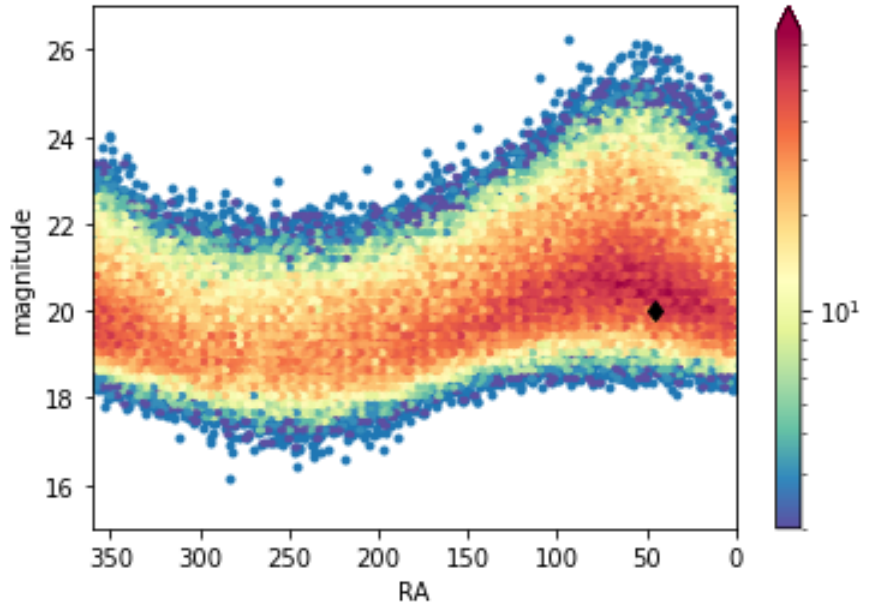

Figure 3.2: The sky density plane, right ascension RA (x-axis) against predicted magnitude h (y-axis). The black dot (45,20) is the most probable position of P9 in agreement with ours data.

3.3 Limits

A previous study of this hypothesis has been made with *Fermi*-LAT (Large Area Telescope), see the figure [3.4]. Its range of observability is different from MAGIC ones, ∼20 MeV to ∼300 GeV. [5]

From the *Fermi*-LAT 8-Year Point Source Catalog, we found that the minimum of flux for 100 GeV is 1.13×10^{-11} photon cm^{-2} s^{-1}, while the maximum value is 1.35×10^{-6} photon cm^{-2} s^{-1}. Error are respectively 5.86 $\times10^{-12}$ photon cm^{-2} s^{-1} and3.95×10^{-8} photon cm^{-2} s^{-1}.[6]

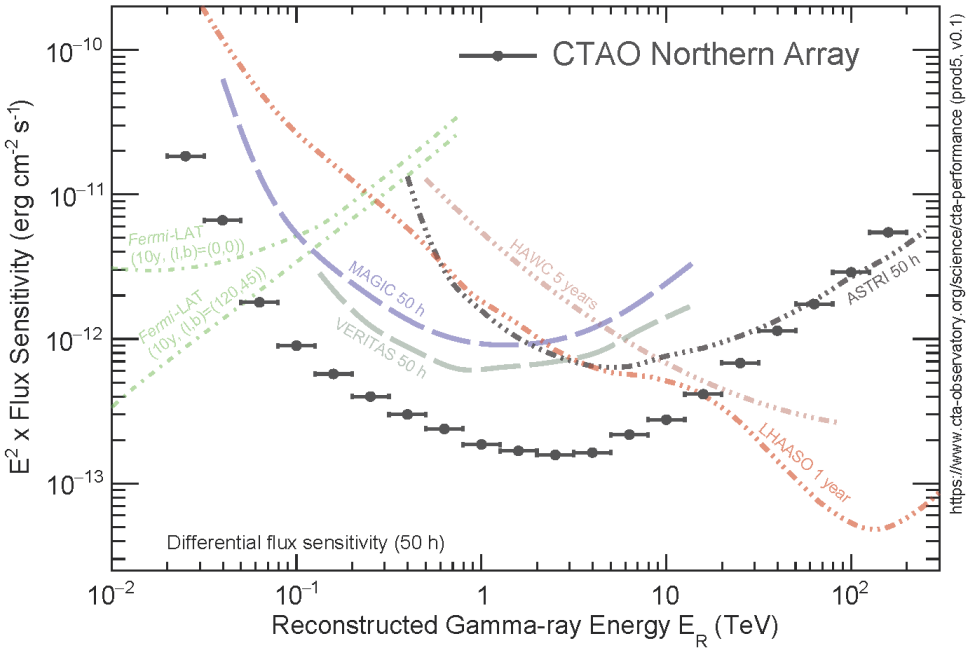

Figure 3.3: Comparison between sensitivity of CTA with other facilities. MAGIC blue dashed line, Fermi LAT green dotted line. The differential sensitivity shown below is defined as the minimum flux needed by CTAO to obtain a 5-standard-deviation detection of a point-like source, calculated in non-overlapping logarithmic energy bins, five per decade. Besides the significant detection, we require at least ten detected gamma rays per energy bin, and a signal/background ratio of at least 1/20. The analysis cuts in each bin have been optimised to achieve the best flux sensitivity to point-like sources. The optimal cut values depend on the duration of the observation.

[5] https://www.cta-observatory.org/

[6] https://fermi.gsfc.nasa.gov/

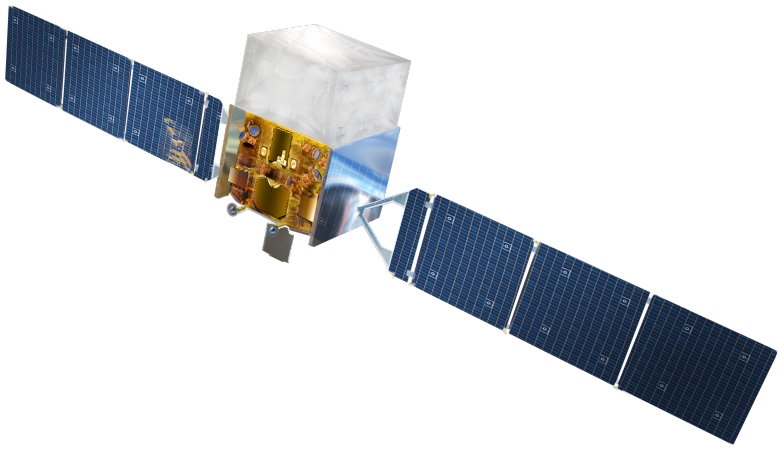

Figure 3.4: *Fermi* Gamma-ray Space Telescope (FGST), the main instrument is Large Area Telescope (LAT) mostly intend to perform an all-sky survey studying astrophysical and cosmological phenomena such high-energy sources and dark matter.

DM annihilation rate

$$\Gamma = 4\pi \int r^2 dr \Big(\frac{\rho(r)}{m}\Big)^2 \langle\sigma v\rangle = \sqrt{\frac{3\rho_{eq}}{8\pi G^3}} \frac{\langle\sigma v\rangle}{m^2} = 10^{20}\mathrm{s}^{-1} \Big(\frac{\langle\sigma v\rangle}{\langle\sigma v\rangle_{ch}}\Big)\Big(\frac{100\mathrm{GeV}}{m}\Big)^2, \tag{3.10}$$

Given the annihilation rate, the flux Φ_γ and the energy flux Φ_E of photons are

$$\Phi_\gamma = \frac{\kappa_1 \Gamma}{4\pi r_9^2} \qquad \Phi_E = \frac{\kappa_2 \Gamma m}{4\pi r_9^2} \tag{3.11}$$

where κ_1 is the average number of photon per DM annihilation within the observable band of the experiment and κ_2 is the fraction of the energy of the DM annihilation converted into photons within the observable energy band. Both depend on the mass and branching annihilation channel of the DM candidate and can be determined. The characteristic bounds are $\kappa_1 \sim 10$ and $\kappa_2 \sim 1$. [7]

The smallest detectable photon flux for *Fermi*-LAT was $\Phi_\gamma = 8.8 \times 10^{-12}$ photon cm^{-2}s^{-1} and the smallest energy flux was $\Phi_E = 5.96 \times 10^{-13}$ photon cm^{-2}s^{-1}. The maximum DM annihilation cross section allowed was

$$\langle\sigma v\rangle < 5.1 \times 10^{-56}\mathrm{cm}^3\mathrm{s}^{-1}\Big(\frac{m}{100\mathrm{GeV}}\Big)^2 \quad (\gamma - \mathrm{flux})$$

$$\langle\sigma v\rangle < 2.2 \times 10^{-55}\mathrm{cm}^3\mathrm{s}^{-1}\Big(\frac{m}{100\mathrm{GeV}}\Big) \quad (\mathrm{E} - \mathrm{flux}).$$

We bound the diffuse gamma ray flux due to PBH Φ_γ by translating the limits on decaying DM with the identification:

$$\frac{d\Phi_\gamma}{dE} \propto \frac{f(1-f^2)\Gamma}{M_{BH}} = \frac{\Gamma_{DM}}{m} \tag{3.12}$$

where m is the mass of decaying DM and Γ_{DM} is the decay rate. [12]

If we consider a mass of 10-10^{6}GeV, the observational limit is

$$\Gamma_{DM} < 10^{-28}\mathrm{s}^{-1}$$

Requiring that the differential flux Γ is less than the limit for f=0.05 implies a bound of

$$\Gamma < 3.7 \times 10^{23} \mathrm{s}^{-1} \Big(\frac{M_{BH}}{5M_{\oplus}} \Big) \Big(\frac{100GeV}{m} \Big)$$

Through the comparison with *Fermi*-LAT and figure [3.3] we can estimate what MAGIC could observe. The picture shows the differential flux sensitivity (50h) for several CTA instruments in energy range 10^{-2}-10^{2} TeV, E^2 Flux Sensitivity (erg $\mathrm{cm}^{-2}\mathrm{s}^{-1}$) against Reconstructed Gamma ray Energy E_R (TeV) [7].
MAGIC (blue dashed line) and *Fermi*-LAT (green dotted line) have roughly the same sensitivity at 10^{-1} TeV (100 GeV). We did not consider other instruments (VERITAS, HAWC, ASTRI, LHAASO) in this thesis. We can assume that MAGIC has more chance to observe this unknown object that can be a PBH because it is the one that has the best sensitivity at the lowest energies.

The observation time by MAGIC telescope at this point, in the range of 22 deg, is 47 h 05 min 35 s (169536 s), we can calculate the limit through the formula

$$limit_{MAGIC} = limit_{Fermi} \times \sqrt{\frac{obs.time_{MAGIC}}{50}}.$$

$$obs.time_{MAGIC} = 47.09 \quad \text{hours}$$

Therefore, limits and bounds for MAGIC are

$$\langle \sigma v \rangle < 4.9 \times 10^{-56} \mathrm{cm}^3 \mathrm{s}^{-1} \Big(\frac{m}{100\mathrm{GeV}} \Big)^2 \quad (\gamma - \mathrm{flux})$$

$$\langle \sigma v \rangle < 2.1 \times 10^{-55} \mathrm{cm}^3 \mathrm{s}^{-1} \Big(\frac{m}{100\mathrm{GeV}} \Big) \quad (\mathrm{E} - \mathrm{flux})$$

$$\Gamma < 3.5 \times 10^{23} \mathrm{s}^{-1} \Big(\frac{M_{BH}}{5M_{\oplus}} \Big) \Big(\frac{100GeV}{m} \Big)$$

[7] https://www.cta-observatory.org/

4. Conclusion and Outlook

We found 11 objects (see Table [1.5]) with 150<a<1000 AU and q>42 AU that are connected with the presence of P9 [15]. To estimate the mass and orbital element it has been used statistical treatment, Markov Chain Monte Carlo. We highlight anomalous orbit of TNOs and OGLE's short microlensing events could have the same origin. Both arise from a PBH of $\sim$ 5-10 $M_\oplus$ as P9. While planets searches use principal optical and infrared/microwave surveys, the signal product by a PBH could be very different [24]. That required dedicated searches for moving sources in X rays, gamma rays, and other high energy cosmic rays.

We fixed the limits for mass and orbital parameter that are mass of $6.2^{+2.2}_{-1.3}$ $M_\oplus$, semimajor axis of 380^{+140}_{-80}AU, perihelion of 300^{+85}_{-60} AU, and inclination of 16$\pm$5 deg. From these, it is possible to find the sky coordinates that are right ascension of $\sim$45deg and declination of $\sim$12 deg (see Figures [3.1] [3.2]), and study an area of celestial sphere of radius $\sim$22 deg around that point. MAGIC telescopes are the best option to search, because their sensitivities are higher and their energy ranges are bigger than other CTAs (see Figures [3.3]) [4][23]. In the hypothesis of PBH we search for DM annihilation signals. We know that the temperature is too low to be detected $\sim$0.0003 K and it is not evaporated yet because the evaporation time is $\sim$50 Gyr, therefore the Hawking radiation is not possible to see. The only way to detect it is by annihilation signals of DM microhalo formed around the PBH. [11].

MAGIC can establish a limit of $\langle\sigma v\rangle_\gamma < 4.9\times10^{-56}\mathrm{cm^3s^{-1}}\left(\frac{m}{100\mathrm{GeV}}\right)^2$ and $\langle\sigma v\rangle_E < 2.1\times 10^{-55}\mathrm{cm^3s^{-1}}\left(\frac{m}{100\mathrm{GeV}}\right)$ using the DL3 observations provided, that correspond to 47.09 hours of total observation. If we use the 15 years of data for MAGIC we will be able to establish limits at the level of $\Gamma < 3.5\times10^{23}\mathrm{s^{-1}}\left(\frac{M_{BH}}{5M_\oplus}\right)\left(\frac{100GeV}{m}\right)$. We note that in the work of [24], they used the all-sky *Fermi*-LAT observations, while we constrained MAGIC observations to a smaller region in the sky, with the consequent loss in sensitivity.

The future work will be to actually search for serendipitous sources in the field of view of the MAGIC observations coincident with these locations using the grid search shown in Figures [2.7,2.8,2.9].

This work can be extended to the recently inaugurated Large Sized Telescope (LST), the first telescope of CTA, that will have a lower energy threshold of 20 GeV.

Bibliography

[1] A. Bouvier; R. Glimore et al. *Prospects of GRB observation for CTA from a phenomenological model*. arXiv:1109.5680v1: ResearchGate, 26 September 2011.

[2] A.A Abdo et al. *Milagro limits and HAWC sensitivity for the rate-density of evaporation Primordial Black Holes*. http://dx.doi.org/10.1016/j.astropartphys.2014.10.007: Elsevier B.V., 5 November 2014.

[3] B. Carr; K. Khri et al. *Constraints on primordial black holes*. arXiv:2002.12778v2: ResearchGate, 9 May 2021.

[4] Bastieri et al. *The MAGIC Telescope and the observation of Gamma Ray Bursts*. 10.1393/ncc/i2005-10136-y: Il nuovo cimento, 28 October 2005.

[5] J. Aleksic et al. *The major upgrade of the MAGIC telescopes, Part II: A performance study using observations of the Crab Nebula*. arXiv:1409.5594v3: Astroparticle Physics, 20 February 2015.

[6] K. Batygin; F.C.Adams et al. *The planet nine hypothesis*. Physics Reports 805 (2019) 1–53: M.P. Kamionkowki, 30 January 2019.

[7] M. Cirelli; G. Corcella et al. *PPPC 4 DM ID: a poor particle physicist cookbook for dark matter indirect detection*. 10.1088/1475-7516/2011/03/051: Journal of Cosmology and Astroparticle Physics, 31 March 2011.

[8] M.L. Ahnen et al. *Limits to dark matter annihilation cross-section from a combined analysis of MAGIC and Fermi-LAT observations of dwarf satellite galaxies*. arXiv:1601.06590v2: JCAP, 16 February 2016.

[9] M.L. Ahnen et al. *Performance of the MAGIC telescope under moonlight*. arXiv:1704.00906v4: Astroparticle Physics, 7 August 2017.

[10] P. Colin et al. *Performance of the MAGIC telescopes insterescopic mode*. arXiv:0907.0960v1: ResearchGate, 6 July 2009.

[11] R. Lopéz-Coto; M. Doro et al. *Prospects for the Observation of Primordial Black Hole evaporation with the Southern Wide Field of View Gamma-ray Observatory*. arXiv:2103.16895v2: ResearchGate, 23 July 2012.

[12] S.M Boucenna; F. Kühnel et al. *Novel constraints on mixed dark-matter scenarios of primordial black holes and WIMPs*. https://doi.org/10.1088/1475-7516/2018/07/003: Journal of Cosmology ans Astroparticle Physics, 2 July 2018.

[13] T.N. Ukawatta; D.R. Stump et al. *Primordial Black Holes: Observation Characteristics of The Final Evaporation*. arXiv:1510.04372v3: ResearchGate, 23 March 2016.

[14] M.E. Brown; K. Batygin. *A search for Planet Nine using Zwicky Transient Facility public archive*. arXiv:2110.13117v1: AAS Journals, 26 October 2021.

[15] M.E. Brown; K. Batygin. *The Orbit of Planet Nine*. arXiv:2108.09868v2: ResearchGate, 22 August 2021.

[16] K. Batygin; M. Brown. *Evidence a giant planet in the solar system*. arXiv:1601.05438v1: ResearchGate, 20 January 2016.

[17] M. Brown. *Planet Nine reference population*. https://data.caltech.edu/records/2098: CaltechDATA, 2 September 2021.

[18] M. Doro; J. Conrad; D. Emmanoulopoulos. *Dark matter and fundamental physics with the Cherenkov Telescope Array*. Astroparticle Physics 43 (2013) 189–214: Elsevier B.V., 25 August 2012.

[19] M. Yu. Khlopov. *Primordial Black Holes*. https://iopscience.iop.org/article/10.1088/1674-4527/10/6/001: RAA, 2 March 2010.

[20] B. Carr; F. Kühnel. *Primordial Black Hole as Dark Matter: Recent Developments*. https://doi.org/10.1146/annurev-nucl-050520- 125911: The Annual Review of Nuclear and Particle Science, 2 August 2020.

[21] Ti-Pei Li; Yu-Qian Ma. *Analysis and result in gamma-ray astronomy*. 10.1086/161295: ResearchGate, 7 February 1983.

[22] A. De Angelis; M. Pimenta. *Introduction to Particle and Astroparticle Physics*. Spinger, 2015.

[23] R.C Gilmore; F. Prada; J. Primack. *Modelling gamma-ray burst observations by Fermi and MAGIC including due to diffuse background light*. 10.1111/j.1365-2966.2009.15909.x: Monthly Notices, 20 October 2019.

[24] J. Scholtz; J. Unwin. *What If Planet 9 Is a Primordial Black Hole?* 10.1103/PhysRevLett.125.051103: Physical review letters, 29 July 2020.